

Evidence for ionised accretion discs in five narrow-line Seyfert 1 galaxies

D. R. Ballantyne^{*}, K. Iwasawa & A. C. Fabian

Institute of Astronomy, Madingley Road, Cambridge CB3 0HA UK

2000 June 1

ABSTRACT

We present the results of fitting *ASCA* spectra of six narrow-line Seyfert 1 (NLS1) galaxies with the ionised reflection models of Ross & Fabian (1993). We find that five of the galaxies (TON S 180, PKS 0558–504, Ark 564, Mrk 335 and PG 1244+026) are well fit by the ionised disc model, and these are often better fits than the alternative models considered. The sixth galaxy, NGC 4051, has additional spectral complexity that cannot be well described by a simple ionised disc model or any of the other alternative models. The highest luminosity NLS1 considered, PKS 0558–504, does not have a well constrained ionisation parameter or reflection fraction. This is because it is difficult to distinguish between highly ionised, highly reflective discs and moderately ionised discs with low reflection fractions. The four galaxies with well constrained fit parameters are consistent with having inclination angles lying between 15 and 30 degrees. Furthermore, these four sources are consistent with having a disc emissivity law that varies as $r^{-2.5}$. These last two properties are also typical of broad-line Seyfert 1 galaxies. We find little or no indication of a correlation between the reflection fraction and the photon index of the underlying continuum. All six of the NLS1s we considered show evidence for a broad Fe $K\alpha$ line, but none of the line centroids are consistent with emission from highly ionised Fe. This is most likely due to the line being redshifted because of relativistic effects. We note that sources with larger ionisation parameters tend to have larger Fe $K\alpha$ EWs. We interpret this as evidence that ionised Fe features are making their presence felt in the spectra. Since most of our sources have steep spectra, highly ionised features are predicted even by the new variable density reflection models. The one source we analyse with a photon index less than two has the lowest ionisation parameter in our sample. We conclude that our result is the strongest evidence yet that NLS1 might have ionised accretion discs. This result gives further weight to the hypothesis that these objects contain rapidly accreting black holes.

Key words: galaxies: active – galaxies: Seyfert – X-rays: galaxies – accretion, accretion discs

1 INTRODUCTION

One of the most basic difficulties in attempting to understand the physics of Active Galactic Nuclei (AGN), is to account for the wide range of properties (i.e., broad lines, radio properties, etc.) that are observed over the whole menagerie of AGN classes. Although it is quite likely that we are observing basically the same phenomenon through different observing angles (e.g., Antonucci 1993), not all AGN can be unified through this picture. Certain classes of AGN seem to be extreme examples of the phenomenon, and cannot fit into the simple unified scheme. It is hoped that such objects would be dominated by one physical property in their cen-

tral engines, and would therefore be simpler to model than a “typical” AGN. An example of this type of extreme AGN is the Narrow Line Seyfert 1 (NLS1) class of galaxies.

NLS1 galaxies, like most AGN, are categorized by their optical emission properties. A NLS1 galaxy has the following characteristics: $\text{FWHM H}\beta < 2000 \text{ km s}^{-1}$, $[\text{O III}]/\text{H}\beta < 3$, and strong Fe II emission (Osterbrock & Pogge 1985). These properties mean that a NLS1 has narrower permitted lines (i.e., broad lines) than a typical Seyfert 1 galaxy. These galaxies also exhibit unusual X-ray properties (Brandt 1999; Leighly 1999a; Leighly 1999b; Vaughan et al. 1999b). In the soft X-ray band (usually taken to mean the *ROSAT* band: 0.1–2.4 keV) these galaxies show very steep spectra due to a significant soft excess, with a power-law photon index (Γ ; where the photon flux $\propto E^{-\Gamma}$) sometimes exceeding

^{*} drb@ast.cam.ac.uk

3 (Boller, Brandt & Fink 1996). In the hard X-ray band, the steep power-law flattens out to a typical $\Gamma \approx 2.1$ – 2.4 (Brandt, Mathur & Elvis 1997; Leighly 1999b; Vaughan et al. 1999b), which is significantly steeper than the spectra of broad-line Seyfert 1 objects. The soft excess is well fit by a model that is suggestive of thermal emission from a disc. NLS1 also exhibit more rapid and extreme variability in the X-ray bands than their broad-line counterparts (Turner et al. 1999; Leighly 1999a).

The model that is currently the most successful in explaining these properties is one which proposes that NLS1 galaxies have smaller black hole masses than typical Seyfert galaxies (e.g., Boller et al. 1996; Laor et al. 1997). This would explain the optical line properties, because the material in the broad line region would have smaller velocities and so their lines will have a smaller Doppler width. However, since these galaxies have about the same luminosity as broad-line Seyfert galaxies, then they must be emitting a higher fraction of their Eddington luminosity. This implies a higher accretion rate and a hotter accretion disc, which would cause the thermal emission of the disc to shift into the soft X-ray band. The steeper high energy Γ could then be explained by Compton cooling of the hard X-ray emitting corona by the soft emission from the disc. The extreme variability would just be a result of the smaller black hole mass because the primary emission region would be smaller; however, it is difficult to rule out the possibility of a beamed component. An analogy between NLS1 and Galactic black hole candidates emitting in their soft/high state has often been stated (e.g., Pounds, Done & Osborne 1995), although its usefulness has been debated.

Hard X-ray observations of NLS1 can test this model. Models of Fe $K\alpha$ line emission at various accretion rates by Matt, Fabian & Ross (1993) have shown that at modest accretion rates, the accretion disc will have an ionised skin on top. This result assumes that the illuminating X-ray flux depends on the accretion rate, which is reasonable if the hard X-ray emitting corona does result from a process like magnetic flaring (e.g., Galeev, Rosner & Vaiana 1979; Haardt, Maraschi & Ghisellini 1994; Svensson 1996). Preliminary evidence for ionised accretion discs based on *ASCA* data has been found in two NLS1 (TON S 180: Comastri et al. (1998) and Turner, George & Nandra (1998); Ark 564: Vaughan et al. (1999a), but see Turner, George & Netzer (1999) for an alternative interpretation). However, these conclusions were made either by estimating the energy centroid of the observed Fe $K\alpha$ line or Fe K edge and ignoring the rest of the continuum, or by using the PEXRIV ionised disc model of Magdziarz & Zdziarski (1995). Ionised reflection has observable effects over the whole continuum, so better constraints on the ionisation state can be made by fitting ionised disc models over the entire observed energy range. However, as shown by Ross, Fabian & Young (1999), the PEXRIV model is inaccurate as the disc becomes highly ionised. A further limitation of this model is that the Fe $K\alpha$ line has to be added in separately.

This paper presents the results of fitting the ionised disc models of Ross & Fabian (1993; hereafter RF) to *ASCA* observations of 6 NLS1 galaxies. These models not only include the Fe $K\alpha$ line, but also spectral features (emission lines and recombination continua) at lower energies. We take advantage of this information by fitting the models over a wide

range of energy. The data selection and reduction procedure is described in Section 2. We briefly outline the properties of our models in Section 3, and then move on to report the results of our fits in Section 4. Finally, we discuss our results in Section 5, and summarise our conclusions in Section 6.

2 OBSERVATIONS AND DATA REDUCTION

A summary of *ASCA* observations of the sample galaxies, as well as other relevant data, is shown in Table 1. The spectral data from the four detectors were reduced from the event files taken from the *ASCA* archive maintained by the *ASCA* Guest Observer Facility (*ASCA* GOF) at NASA/Goddard Space Flight Center, using FTOOLS 4.2 and the standard calibration. Source photons were collected from a region with a radius of typically 4 arcmin for the Solid state Imaging Spectrometer (SIS; S0 and S1) and 5 arcmin for the Gas Imaging Spectrometer (GIS; G2 and G3), while background data were taken from a source-free region on the detectors in the same observations. All the targets show significant X-ray variability during the observations. The *ASCA* light curves of our sample galaxies have been published elsewhere (Leighly 1999a). We present a spectral analysis of time-averaged data of individual sources integrated over each observation.

The SIS was operating with 2CCD chips switching between Faint and Bright modes for the observations of Mrk 335 and PG 1244+026. The Faint mode data of these observations have been converted to the Bright mode format to add together with the original Bright mode data. For the others, the SIS was operating with 1CCD Faint mode throughout. These Faint mode data have been converted to a format called “Bright2” for analysis.

Response matrices for the SIS were generated by SISRMG version 1.1. Version 4.0 matrices provided by the GIS team were used for the GIS. The effective areas of the source spectra were computed with ASCAARF version 2.73. For observations carried out after 1994, the efficiency of the SIS, typically in the energy range below 1 keV, has been noticed to be decreasing continuously. Since the correction for this effect has not been implemented in ASCAARF at this stage, the effective area of the SIS in the low energy range is likely to be overestimated for some targets in our sample. We therefore restrict our spectral analysis to the energy range above 1 keV, except the data for Mrk 335 and NGC 4051 which were observed when the SIS degradation was insignificant.

3 IONISED DISC MODEL

We employed the ionised disc models described in detail by RF and Ross et al. (1999), and so we will only give a brief outline here. A slab of gas consisting of solar Morrison & McCammon (1983) abundances, and with a constant hydrogen number density of $n_H = 10^{15} \text{ cm}^{-3}$, is illuminated by an X-ray power-law with flux F_x (defined over 0.01–100 keV) and photon index Γ . The computed reflection spectrum is then multiplied by a factor R , where R is the reflected fraction, and then added to the illuminating spectrum to find the model observed spectrum.

Table 1. Summary of *ASCA* observations and other relevant properties of the sample galaxies. N_H is the Galactic absorbing column in units of 10^{20} cm^{-2} , and L_{2-10} is the 2–10 keV luminosity in units of 10^{43} ergs s^{-1} (assuming $H_0=50$ km s^{-1} Mpc^{-1}).

Galaxy	z	Date	SIS mode	Exposure ¹ SIS/GIS (ks)	Count rate (1–10 keV) ² SIS/GIS (cps)	N_H^a	L_{2-10}^a	<i>ROSAT</i> Γ^a
Mrk 335	0.025	1993 Dec 9	2CCD Faint/Bright	25.1/20.4	0.475/0.294	1.50	8.9	3.04
NGC 4051	0.0024	1994 Jun 7–9	1CCD Faint	81.7/71.1	0.854/0.472	1.31	0.056	2.84
PG 1244+026	0.048	1996 Jul 1–3	2CCD Faint/Bright	49.6/38.8	0.165/0.085	1.93	2.62	3.26
TON S 180	0.062	1996 Jul 10–11	1CCD Faint	54.2/49.2	0.306/0.158	1.50	8.9	3.04
Ark 564	0.024	1996 Dec 23–24	1CCD Faint	54.8/50.8	1.329/0.657	6.40	5.5	3.47
PKS 0558–504	0.137	1996 Sep 5–6	1CCD Faint	44.3/34.4	0.660/0.359	4.39	124	2.89

¹ Good exposure time of single detector of each type.

² Mean count rate in the 1–10 keV band obtained from the S0 (for the SIS) and G2 (for the GIS) detectors.

^a data taken from Leighly (1999b).

The important quantity in determining the structure of the reflected spectrum is the ionisation parameter,

$$\xi = \frac{4\pi F_x}{n_H}. \quad (1)$$

The larger ξ is, the more ionised the gas is, and this will affect the strength and width of the features in the reflected spectrum like the Fe $K\alpha$ line and the various absorption edges (Matt et al. 1993, 1996).

We computed a three-dimensional grid of models with $0.0 \leq R \leq 2.0$, $1.7 \leq \Gamma \leq 3.0$, and $1.0 \leq \log \xi \leq 6.0$. The ionisation parameter was varied by changing only the incident flux. We did not include the influence of soft radiation from the disc itself, but since we are mainly dealing with energies greater than 1 keV (Sections 2 & 4.1), this should not be an important effect.

There are some important deficiencies in the RF models. Foremost among them is the assumption of constant density in the reflecting slab. Recently, Nayakshin, Kazanas & Kallman (2000) presented ionised reflection models where hydrostatic equilibrium is solved along with the ionisation and radiation structure. They find that, due to a thermal instability, only a very thin layer (with Thomson optical depth, $\tau_t \lesssim 1$) at the top of the slab is highly ionised, and the reflection spectrum is dominated by the cool, neutral material underneath. If this is the case, then it would be inappropriate to fit data with the reflection spectra predicted by constant density models, such as the RF model used here, because they predict the presence of highly ionised features. However, all is not lost, because the models of Nayakshin et al. (2000) show that if the disc is radiation pressure dominated and the illuminating power-law has $\Gamma \gtrsim 2$ then ionised features can be seen in the reflection spectrum. In that case, our fits to these NLS1 sources might be reasonable because most of them have $\Gamma > 2$. Evidence for this interpretation is presented in Section 5.

4 RESULTS

4.1 Spectral fitting

Data from all four detectors were used in the spectral fitting. However, as mentioned in Section 2, the SIS detectors' efficiency below 1 keV has slowly been degrading since late 1994. This is not corrected by the data reduction software and could lead to inaccuracies in determining continuum properties. Moreover, the sensitivity of the GIS detectors

falls off sharply around 1 keV. To deal with these issues we adopted the following conservative approach. If an observation was made after 1994 we determined if there was any discrepancy in fit residuals between the SIS and GIS detectors below 2 keV. If there was we used the GIS data down to 1 keV and the SIS data only where the two agreed. If there was no visible discrepancy, both the GIS and SIS data was used down to 1 keV. If data was taken before late 1994 then the low energy SIS data may be used, but we made sure it was consistent with the GIS data. In all cases we used data up to 10 keV. The only exception to this was Ark 564, where we used simultaneous *RXTE* data kindly provided by S. Vaughan. This data was processed as in Vaughan et al. (1999a), except we used data from all 5 of the satellite's Proportional Counter Units. To avoid calibration and background uncertainties we only fit these data between 3 and 20 keV. Finally, we have noticed that the S0 data of Ark 564 are inconsistent in the energy range above 4 keV with the other four detectors which are in good agreement with each other. Since applying even more careful data selection than the normal practice could not eliminate the problem, we attribute it to some anomaly in the detector. We therefore use only the S0 data below 4 keV in this particular data set.

We used XSPEC v11.0 for the spectral fitting. The grid of ionised disc models that was computed (Section 3) was converted into a tablefile that could be read in by XSPEC. In each fit, we let the relative normalisation between the SIS and the GIS vary, but we fixed the cold absorption at the Galactic value. Since we primarily fit data with energies greater than 1 keV, any excess absorption within a particular galaxy will not greatly affect our results. For each galaxy we fit its spectrum two different ways using the ionised disc models. First, we fit the data using just the model spectrum. Second, we included the effects of relativistic smearing by blurring the model with the Laor (1991) kernel for the Kerr metric. This blurring has four parameters: the inner radius of the emitting annulus (r_{min}), the outer radius of the annulus, the exponent of the surface emissivity law (assumed to go as r^α), and the inclination of the disc along the line of sight. The outer radius was fixed to be at $1000 r_g$, where $r_g = GM/c^2$ is the gravitational radius, (the actual value of this parameter will not affect the fit as the blurring effects come from the inner regions of the annulus), and the inclination angle was fixed at 30 degrees which is typical for Seyfert 1 galaxies (Nandra et al. 1997a). We then fit the data with the models using four different combinations of r_{min} and α :

$(r_{min}, \alpha) = (10, -2.0; 10, -2.5; 6, -2.0; 6, -2.5)$, where r_{min} is given in units of gravitational radii. Finally, using the best fitting model of the four considered, we fit the inclination angle.

When the ionised disc models were blurred it was necessary for energies outside the response matrix of the detector to be used in order to avoid effects at the edges of the observed energy range. This was done by using the ‘extend’ command in XSPEC to extend the energy range of the response matrix. As long as edge effects were avoided, the results of the fits do not depend on how far we extended the response matrix.

The results of these fits are shown in Table 2 and in Figures 1–6. Plots of the ratio of the data to a simple absorbed power-law model can be seen elsewhere (Leighly 1999b). Note that all the spectra in Figs. 1–6 are plotted in the observed frame, while all the fit parameters are quoted in the rest frame. The errors reported in Table 2 and in all subsequent tables correspond to a 90 per cent confidence interval for one interesting parameter.

To determine the Fe $K\alpha$ line parameters of the galaxies, we fit the spectra above 3 keV with a simple absorbed power-law model. To obtain a good estimate of the photon index, Γ , we ignored the data between 5 and 7 keV (observed frame) to avoid the influence of the Fe $K\alpha$ line. Once we obtained the best-fitting value of Γ , we fixed it at that value and fit a Gaussian profile to the Fe $K\alpha$ line. The energy centroid of the Gaussian was constrained to lie between 5.5 and 7.5 keV, and its width (σ) between 0 and 2 keV. The rest frame fit parameters are shown in Table 3. Despite the differences in data reduction and analysis methodology, our values compare well with previously published results (e.g., Leighly 1999b; Vaughan et al. 1999b).

As a check on the relative importance of our ionised disc fits we also fit the spectra with three alternative models: a simple power-law plus gaussian line model, the warm absorber ABSORI model (Done et al. 1992; Zdziarski et al. 1995), and the ionised disc PEXRIV model. The latter two models are included in the XSPEC package. The Fe $K\alpha$ line parameters that were found earlier were included in these fits but were fixed at their best-fitting values. The results of these fits are shown in Table 4. The displayed values of ξ have been corrected for the different energy range in their definition, and so can be compared with the values in Table 2. The ABSORI models were run with the temperature of the absorber fixed at 10^6 K, and with solar Fe abundance (adjusted to match the abundances used in the RF models). Similarly, the PEXRIV models had the disc temperature fixed at 10^6 K, the inclination angle fixed at 30 degrees, and solar abundances (after correction). The power-law cutoff energy for the PEXRIV models was fixed at 100 keV, in agreement with our models.

4.2 Interpretation of the spectral fitting results

Studying the results listed in Tables 2–4 gives rise to the following comments:

(i) The RF ionised disc model provides an adequate fit to the *ASCA* data in five out of the six sources examined. The only source that the model does not fit is NGC 4051, which contains a warm absorber and is well known for its spectral

complexity (Guainazzi et al. 1996). An attempt to fully account for all the features in the spectrum of NGC 4051 is beyond the scope of this paper.

(ii) In general, the alternative models presented in Table 4 have difficulty fitting the data with realistic values of the parameters. These models seem to be able to fit the data only with a large value of the photon index, Γ . If Γ is fixed at the value determined from the 3–10 keV fits, then the fits are quite poor and often results in an extremely small Fe $K\alpha$ EW. This is because of the unrealistically strong Fe K edge one finds in the ABSORI and PEXRIV models (e.g. Ross et al. 1999). The RF models determine a value of Γ that is comparable with the ones determined from the high energy fit, and so does a good job matching the intrinsic continuum shape.

(iii) The RF results show that the accretion discs in these sources might be relatively highly ionised with $\xi > 1500$; however, the values determined by ABSORI and PEXRIV are usually too low and poorly constrained. Furthermore, these models can only reach a maximum ξ of 3200, and so are not capable of fitting highly ionised sources.

(iv) The RF fit for the high luminosity source PKS 0558–504 is not well constrained in $R - \xi$ space (see the lower-right panel in Fig. 2). This is because it is difficult to tell the difference between a highly reflective, highly ionised disc and a moderately ionised disc with a low reflection fraction. In Table 2 we list fits for this source when the reflection fraction is free and when it is fixed at unity. Both cases give good fits to the data. We will use the parameters from the fit when R was free in later discussions, but the above degeneracy should be kept in mind. One possible way to break this degeneracy is to search for ionised edges and lines in the soft X-ray band. These features should be present in a spectrum from a moderately ionised disc, even with a low reflection fraction. They would not be present at all from a highly ionised reprocessor. Obviously, the data would need to have extremely good signal-to-noise to detect these features and rule out alternatives such as warm absorbers.

(v) The four sources which have well constrained RF fits all have inclination angles between 15 and 30 degrees which contradict some earlier results (Ark 564: Turner, George & Netzer 1999). These are consistent with the inclination angles of broad-line Seyfert 1 galaxies (Nandra et al. 1997a). Fits to PKS 0558–504 result in large inclination angles. However, the PKS 0558–504 Fe $K\alpha$ line is quite noisy, so those inclinations are quite suspect.

(vi) None of the Fe $K\alpha$ lines have centroid energies that are consistent with coming from highly ionised iron. However, this does not mean that ionised Fe is not present in the data, because the lines will be redshifted due to relativistic blurring effects. Again, the noisiness of the PKS 0558–504 Fe $K\alpha$ line did not allow precise measurements of the line parameters.

(vii) Aside from PKS 0558–504, all the sources are best fit with a disc emissivity law that is proportional to $r^{-2.5}$, consistent with the results of Nandra et al. (1997a). Also, most of the sources are consistent with the emission occurring inwards of $10 r_g$. However, it should be emphasized that we didn’t fit for α and r_{min} , we just considered four different cases.

Table 2. Best fit parameters of the RF ionised disc models. All values are quoted in the rest frame. Γ is the photon index, ξ is the ionisation parameter as defined in Equation 1, R is the reflection fraction, r_{min} is the inner radius of the emitting annulus in units of r_g , α is the exponent for the disc emissivity law, and i is the inclination of the disc to the line of sight in degrees.

Galaxy	Model	Energy Range ^a	Γ	$\log \xi$	R	r_{min}	α	i	χ^2/dof	χ^2_{red}
TON S 180	not blurred	1–10	2.48±0.02	3.30 ^{+0.33} _{-0.07}	0.922 ^{+0.132} _{-0.221}				834/860	0.970
	blurred		2.44	3.54	1.041	10.0	-2.0	30.0 ^f	829/860	0.964
			2.45	3.55	1.136	10.0	-2.5	30.0 ^f	824/860	0.958
			2.44	3.55	1.096	6.0	-2.0	30.0 ^f	827/860	0.962
			2.46±0.02	3.58 ^{+0.13} _{-0.07}	1.22 ^{+0.32} _{-0.24}	6.0	-2.5	30.0 ^f	823/860	0.957
PKS 0558–504	not blurred	1–10	2.48 ^{+0.02} _{-0.03}	3.60 ^{+0.11} _{-0.09}	1.205 ^{+0.264} _{-0.239}	6.0	-2.5	21.8 ^{+8.1} ₋₁₆	820/859	0.955
			2.27 ^{+0.02} _{-0.01}	3.69 ^{+0.51} _{-0.44}	0.165 ^{+0.113} _{-0.069}				1022/1054	0.970
			2.27±0.02	3.68 ^{+0.51} _{-0.38}	0.198 ^{+0.172} _{-0.083}	10.0	-2.0	30.0 ^f	1022/1054	0.970
			2.27	3.60	0.184	10.0	-2.5	30.0 ^f	1023/1054	0.971
			2.27	3.60	0.187	6.0	-2.0	30.0 ^f	1023/1054	0.970
	blurred		2.27	3.60	0.167	6.0	-2.5	30.0 ^f	1027/1054	0.974
			2.26±0.02	3.85 ^{+0.23} _{-0.12}	0.431 ^{+0.183} _{-0.162}	10.0	-2.0	89.4 ^{+0.6p} _{-35.5}	1016/1053	0.965
		not blurred	2.25±0.02	4.48 ^{+0.27} _{-0.16}	1.0 ^f				1032/1055	0.979
		blurred	2.25 ^{+0.02} _{-0.01}	4.48 ^{+0.26} _{-0.23}	1.0 ^f	10.0	-2.0	30.0 ^f	1031/1055	0.978
			2.25	4.48	1.0 ^f	10.0	-2.5	30.0 ^f	1036/1055	0.982
			2.25	4.48	1.0 ^f	6.0	-2.0	30.0 ^f	1033/1055	0.980
			2.25	4.48	1.0 ^f	6.0	-2.5	30.0 ^f	1042/1055	0.988
	2.25 ^{+0.01} _{-0.02}	4.17 ^{+0.19} _{-0.15}	1.0 ^f	10.0	-2.0	89.9 ^{+0.1p} _{-28.3}	1019/1054	0.966		
Ark 564	not blurred	1–20	2.59±0.01	3.38 ^{+0.13} _{-0.04}	0.520 ^{+0.054} _{-0.044}				1399/1337	1.046
			blurred	2.59	3.39	0.530	10.0	-2.0	30.0 ^f	1377/1337
	blurred		2.59	3.40	0.564	10.0	-2.5	30.0 ^f	1368/1337	1.023
			2.59	3.40	0.540	6.0	-2.0	30.0 ^f	1374/1337	1.028
			2.59±0.01	3.40 ^{+0.15} _{-0.05}	0.602 ^{+0.054} _{-0.103}	6.0	-2.5	30.0 ^f	1367/1337	1.022
	2.59±0.01	3.41 ^{+0.14} _{-0.05}	0.607 ^{+0.056} _{-0.050}	6.0	-2.5	27.4 ^{+2.4} _{-5.1}	1364/1336	1.021		
NGC 4051	not blurred	0.5–10	1.82±0.01	3.39±0.01	2.0 ^{+0.0p} _{-0.17}				2627/1833	1.433
			blurred	1.85	3.18	1.02	10.0	-2.0	30.0 ^f	2589/1833
	blurred		1.85	3.19	1.10	10.0	-2.5	30.0 ^f	2445/1833	1.334
			1.85	3.18	1.04	6.0	-2.0	30.0 ^f	2528/1833	1.379
			1.85±0.01	3.198±0.004	1.21 ^{+0.08} _{-0.06}	6.0	-2.5	30.0 ^f	2349/1833	1.281
			1.86±0.01	3.200 ^{+0.004} _{-0.003}	1.19 ^{+0.07} _{-0.05}	6.0	-2.5	21.6 ^{+3.0} _{-2.9}	2351/1832	1.283
Mrk 335	not blurred	0.6–10	1.98±0.02	3.34 ^{+0.06} _{-0.07}	0.678 ^{+0.217} _{-0.137}				800/733	1.091
			blurred	1.98	3.27	0.763	10.0	-2.0	30.0 ^f	797/733
	blurred		1.98	3.26	0.836	10.0	-2.5	30.0 ^f	788/733	1.076
			1.98	3.26	0.792	6.0	-2.0	30.0 ^f	793/733	1.082
			1.98±0.02	3.25±0.10	0.888 ^{+0.197} _{-0.180}	6.0	-2.5	30.0 ^f	785/733	1.071
	1.99±0.02	3.28 ^{+0.11} _{-0.12}	0.876 ^{+0.112} _{-0.165}	6.0	-2.5	21.0 ^{+8.5} _{-11.9}	782/732	1.068		
PG 1244+026	not blurred	1–10	2.43±0.04	3.91 ^{+0.28} _{-0.39}	1.44 ^{+0.56p} _{-0.48}				544/517	1.052
			blurred	2.41	3.86	1.83	10.0	-2.0	30.0 ^f	544/517
	blurred		2.42 ^{+0.04} _{-0.03}	3.86 ^{+0.26} _{-0.29}	1.89 ^{+0.11p} _{-0.69}	10.0	-2.5	30.0 ^f	543/517	1.050
			2.41	3.85	1.89	6.0	-2.0	30.0 ^f	543/517	1.051
			2.43	3.85	1.88	6.0	-2.5	30.0 ^f	544/517	1.052
	2.44±0.04	3.76 ^{+0.37} _{-0.19}	1.46 ^{+0.54p} _{-0.48}	10.0	-2.5	15.2 ^{+13.6} _{-15.2p}	540/516	1.046		

^a units of keV

^f parameter fixed at value

^{p/p} parameter pegged at upper/lower limit

5 DISCUSSION

The chief advantage of the RF model over the PEXRIV model is that it fits the Fe K α line and the continuum simultaneously, as they are both computed together. Since the Fe K α line is often the most significant deviation in an otherwise featureless power-law spectrum, this ability to fit both components together is a significant improvement. This is best illustrated by noting that the RF models find a value of Γ that is consistent with the value computed using only high

energy data, whereas models like PEXRIV and ABSORI find significantly larger values.

We can now use our results to compare with ones derived from simpler models. One of these results is an apparent correlation between the reflection fraction R , and the photon index Γ , such that objects with larger photon indices have larger reflection fractions (Zdziarski, Lubiński & Smith 1999). In Figure 7 we plot R versus Γ for the best fitting blurred RF models (excluding NGC 4051, but including the free- R fit of PKS 0558–504). This figure shows that any correlation between R and Γ must be very weak.

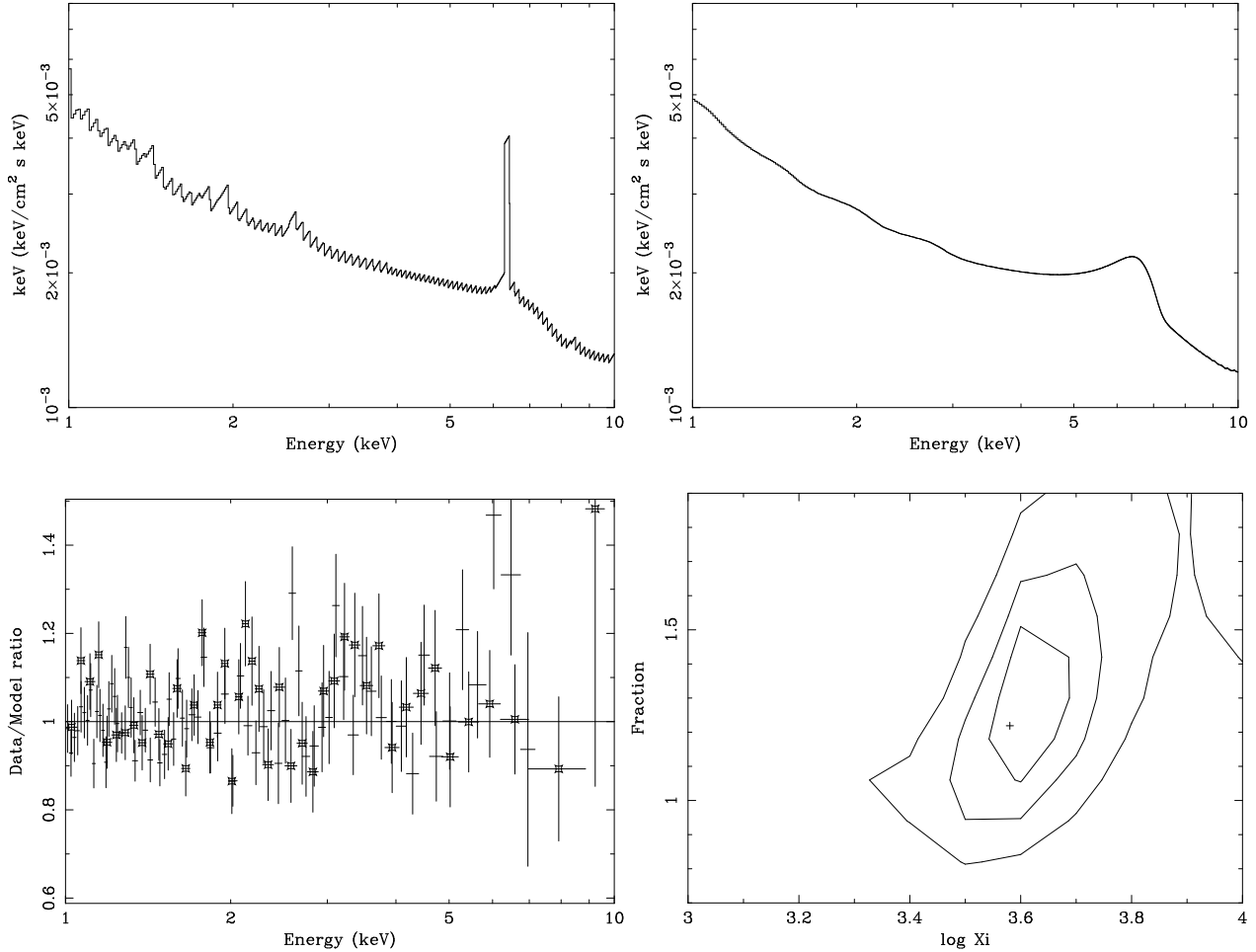


Figure 1. Results from fitting TON S 180 with the RF ionised disc model. The top-left figure shows the best fit unblurred model: $\Gamma = 2.48$, $\log \xi = 3.30$, and $R = 0.922$. The top-right panel shows the best fit relativistically blurred model when $i = 30$ degrees: $\Gamma = 2.46$, $\log \xi = 3.58$, $R = 1.22$, $r_{min} = 6 r_g$, and $\alpha = -2.5$. The bottom left panel displays the ratio of the data to the best blurred model from the top right panel. Here, only the S0 data (no symbols) and the G2 data (open symbols) have been rebinned and plotted. Finally, the bottom right panel shows the 68, 90 and 99 per cent confidence contours around the best fitting blurred model shown in the top right panel. The position of the best fit model is denoted by the plus sign.

However, it should be noted that the correlation pointed out by Zdziarski et al. (1999) was mainly for sources with hard spectra; they did not have many sources with $\Gamma > 2$.

It was mentioned in Section 3 that the constant density RF models might not be inconsistent with the results of the variable density models of Nayakshin et al. (2000) when $\Gamma > 2$. Evidence for this interpretation is presented in Figure 8, which plots $\log \xi$ of the best fit blurred RF models (when the inclination was fixed at 30 degrees) of our sample versus the equivalent width of the Fe K α line that was computed from the high energy power-law plus gaussian fits. This figure shows a general trend that more highly ionised sources have larger Fe K α equivalent width. This is a typical prediction of constant density models (e.g. Matt et al. 1993): as the top of the disc becomes more ionised, emission from highly ionised Fe at 6.7 and 6.9 keV will become visible and this will increase the equivalent width of the line. Recall that most of our sources have relatively low 2–10 keV luminosities (Table 1), and so we should not observe (and, indeed, we do not) a decrease in Fe K α EW with luminos-

ity which is seen in higher luminosity sources (the so-called X-ray Baldwin effect; Iwasawa & Taniguchi 1993; Nandra et al. 1997b). If our sources all had flat spectra ($\Gamma \lesssim 2$) then the trend seen in Figure 8 would be cause for concern; however, only one of our sources has $\Gamma < 2$ (plotted with the open symbol in Figure 8) and this source has the smallest ionisation parameter in our sample, consistent with the results of Nayakshin et al. (2000). The rest of the sources have $\Gamma > 2$ and have larger ionisation parameters. Therefore, we conclude that our results are not inconsistent with the results of Nayakshin et al. (2000) despite our use of constant density models.

One other limitation of the models used in this paper is the restriction to solar abundance. There is no reason *a priori* to expect that the abundances in accretion discs to be solar, but, then again, there is no strong evidence that they are not solar. Changing the abundances has the greatest effect on the Fe K α line, but, given the poor signal-to-noise in most of the observations presented above, disentangling this effect from the other ones would be quite difficult. Hope-

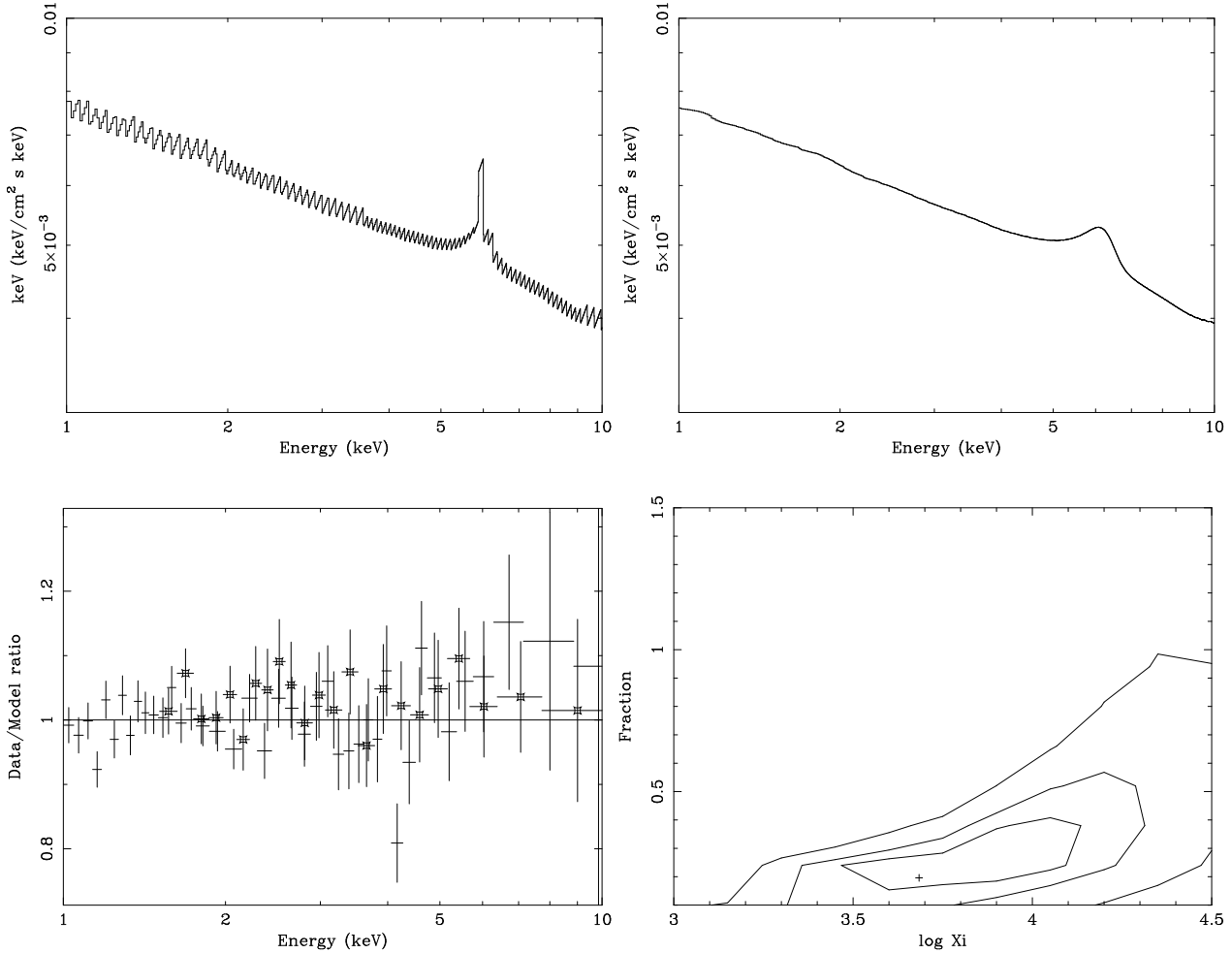


Figure 2. Results from fitting PKS 0558–504 with the RF ionised disc model. The top-left figure shows the best fit unblurred model: $\Gamma = 2.27$, $\log \xi = 3.69$, and $R = 0.165$. The top-right panel shows the best fit relativistically blurred model when $i = 30$ degrees: $\Gamma = 2.27$, $\log \xi = 3.68$, $R = 0.198$, $r_{min} = 10 r_g$, and $\alpha = -2.0$. The bottom left panel displays the ratio of the data to the best blurred model from the top right panel. Here, only the S0 data (no symbols) and the G2 data (open symbols) have been rebinned and plotted. Finally, the bottom right panel shows the 68, 90 and 99 per cent confidence contours around the best fitting blurred model shown in the top right panel. The position of the best fit model is denoted by the plus sign.

fully, higher signal-to-noise observations by *XMM-Newton* and *Chandra* will help constrain the abundances in accretion discs.

6 CONCLUSIONS

We have fit *ASCA* observations of six NLS1 galaxies with the ionised disc models of RF, and found that five of the sources are well fit by such a model. The only source that was not well fit by the ionised disc model was the complicated source NGC 4051. The ionisation parameter and reflection fraction of the highest luminosity source, PKS 0558–504, were not well constrained by the models. This is because the models suffer from a degeneracy between high R , high ξ discs and low R , low ξ discs. Observations with higher signal-to-noise in the soft X-ray band might be able to break this degeneracy.

The four well constrained sources all have inclination angles typical of broad-line Seyfert 1 galaxies (between 15

and 30 degrees), and are consistent with most of the emission coming from inside $10 r_g$. We find only a very weak or nonexistent correlation between the reflection fraction and the photon index.

While our models make the rather large simplifying assumption that the density of the disc is constant, because most of the sample sources have steep spectra and will therefore show ionised features in their reflection spectra (predicted from the non-constant density models of Nakashin et al. 2000), our results are probably not unreasonable. Indeed, the source with the flattest spectrum has the lowest ionisation parameter in the sample and a small Fe K α EW.

These results are the strongest evidence yet that NLS1 galaxies might possess ionised discs. This improvement comes about because the RF models include the Fe K α line emission, can handle large ionisation parameters, and we fit a large energy range (typically 1–10 keV). Another ionised disc model, PEXRIV, was usually the best out of the alternative models considered, but had difficulty fitting the contin-

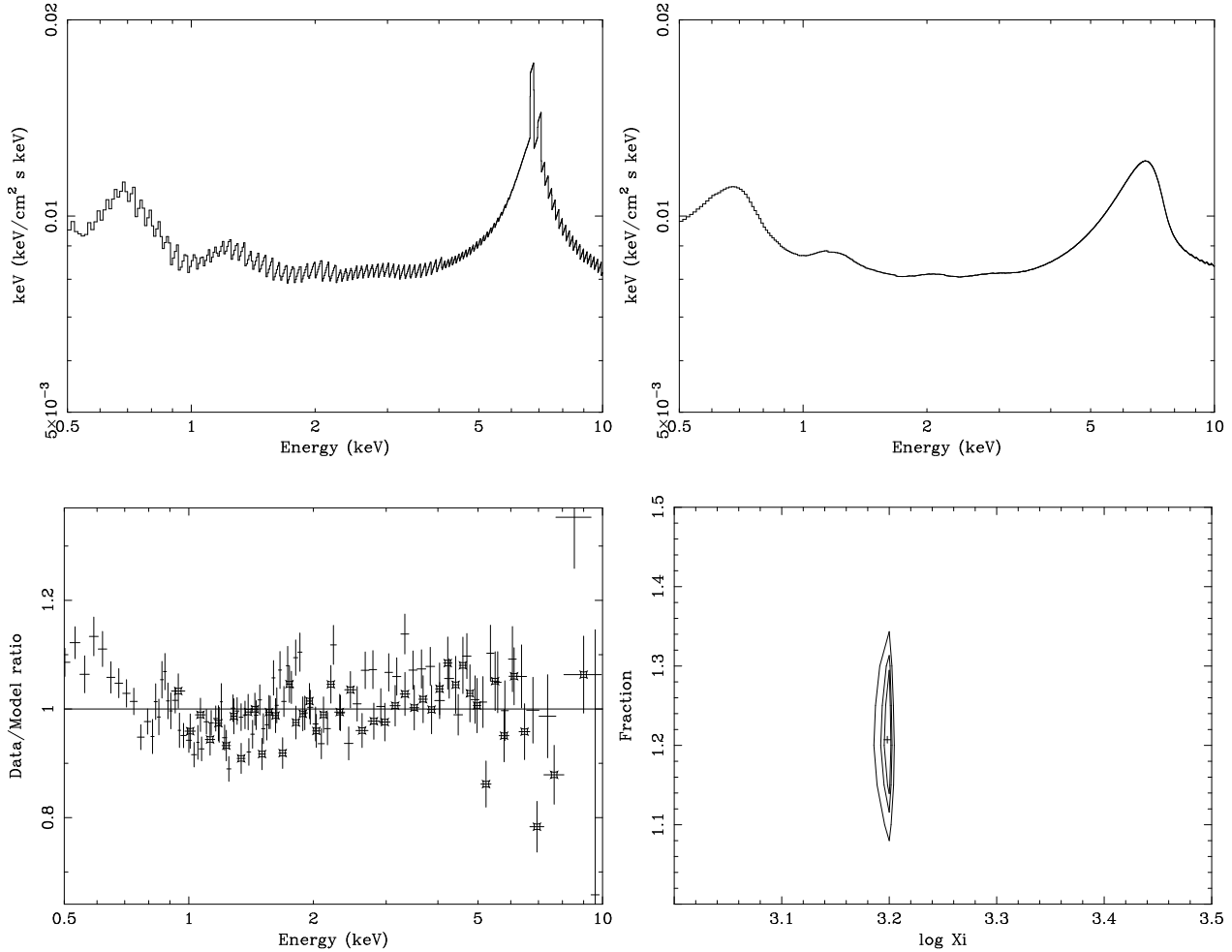


Figure 3. Results from fitting NGC 4051 with the RF ionised disc model. The top-left figure shows the best fit unblurred model: $\Gamma = 1.82$, $\log \xi = 3.39$, and $R = 2.0$. The top-right panel shows the best fit relativistically blurred model when $i = 30$ degrees: $\Gamma = 1.85$, $\log \xi = 3.198$, $R = 1.21$, $r_{min} = 6 r_g$, and $\alpha = -2.5$. The bottom left panel displays the ratio of the data to the best blurred model from the top right panel. Here, only the S0 data (no symbols) and the G2 data (open symbols) have been rebinned and plotted. Finally, the bottom right panel shows the 68, 90 and 99 per cent confidence contours around the best fitting blurred model shown in the top right panel. The position of the best fit model is denoted by the plus sign.

uum and typically underestimated the ionisation parameter. The PEXRIV model is not appropriate to fit possibly highly ionised sources like NLS1 galaxies. These results bolster the claim that the unique properties of NLS1 are driven by relatively low mass black holes accreting at a high fraction of their Eddington rate.

ACKNOWLEDGMENTS

We thank S. Vaughan for providing the *RXTE* data on Ark 564, and R. Ross for advice and useful discussions. DRB acknowledges financial support from the Commonwealth Scholarship and Fellowship Plan and the Natural Sciences and Engineering Research Council of Canada. KI and ACF acknowledge support from PPARC and the Royal Society, respectively. This research has made use of data obtained through the High Energy Astrophysics Science Archive Research Center Online Service, provided by the NASA/Goddard Space Flight Center.

REFERENCES

- Antonucci R., 1993, *ARA&A*, 31, 473
 Boller Th., Brandt, W.N., Fink H.H., 1996, *A&A*, 305, 53
 Brandt W.N., Mathur S., Elvis M., 1997, *MNRAS*, 285, L25
 Brandt W.N. 1999, in Poutanen J., Svensson R., eds, *ASP Conference Series Vol. 161, High Energy Processes in Accreting Black Holes*, Astron. Soc. Pac. San Francisco, p. 166
 Comastri A. et al. 1998, *A&A*, 333, 31
 Done C., Mulchaey J.S., Mushotzky R.F., Arnaud K.A., 1992, 395, 275
 Galeev A.A., Rosner R., Vaiana G.S., 1979, *ApJ*, 229, 318
 Guainzzi M., Mihara T., Otani C., Matsuoka M., 1996, *PASJ*, 48, 781
 Haardt F., Maraschi L., Ghisellini G., 1994, *ApJ*, 432, L95
 Iwasawa K., Taniguchi Y., 1993, *ApJ*, 413, L15
 Iwasawa K., Kunieda H., Awaki H., Koyama K., 1993, *PASJ*, 45, 71
 Laor A., 1991, *ApJ*, 376, 90
 Laor A., Fiore F., Elvis M., Wilkes B.J., McDowell J.C., 1997, *ApJ*, 477, 93
 Leighly K.M., 1999a, *ApJS*, 125, 297

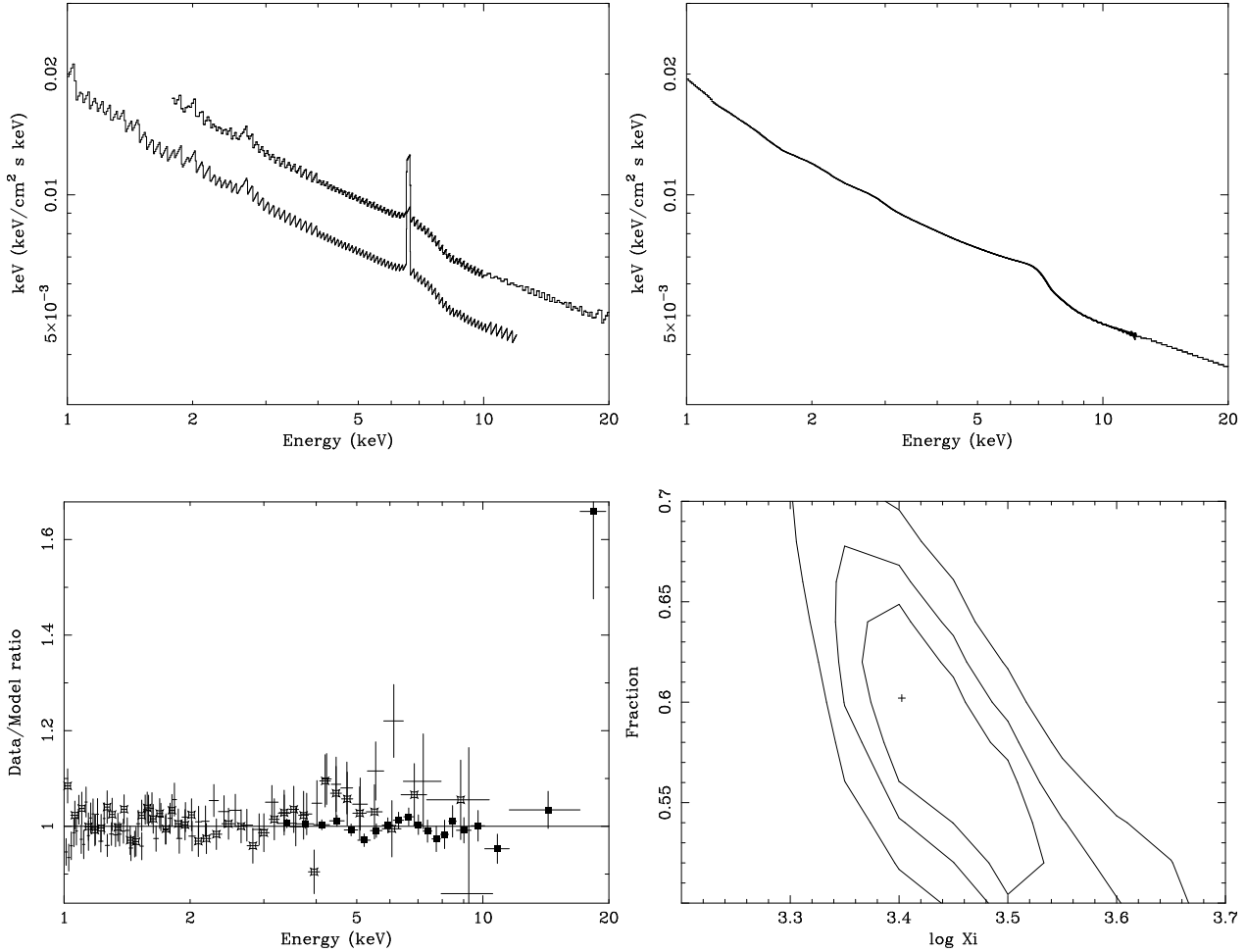


Figure 4. Results from fitting Ark 564 with the RF ionised disc model. The top-left figure shows the best fit unblurred model: $\Gamma = 2.59$, $\log \xi = 3.38$, and $R = 0.520$. The upper curve shows the model through the *RXTE* response matrix, and the lower curve shows the model through the *ASCA* response matrix. The top-right panel shows the best fit relativistically blurred model when $i = 30$ degrees: $\Gamma = 2.59$, $\log \xi = 3.40$, $R = 0.602$, $r_{min} = 6 r_g$, and $\alpha = -2.5$. Here, since the energy range of the response matrices were extended to do the relativistic blurring, only one curve is displayed. The bottom left panel displays the ratio of the data to the best blurred model from the top right panel. Here, the S1 data (no symbols), the *RXTE* data (solid symbols), and the G2 data (open symbols) have been rebinned and plotted. Near 20 keV the data is becoming dominated by the background. Finally, the bottom right panel shows the 68, 90 and 99 per cent confidence contours around the best fitting blurred model shown in the top right panel. The position of the best fit model is denoted by the plus sign.

Leighly K.M., 1999b, *ApJS*, 125, 317
 Magdziarz P., Zdziarski A.A., 1995, *MNRAS*, 273, 837
 Matt G., Fabian A.C., Ross R.R., 1993, *MNRAS*, 262, 179
 Matt G., Fabian A.C., Ross R.R., 1996, *MNRAS*, 280, 823
 Morrison R., McCammon D., 1983, *ApJ*, 270, 119.
 Nandra K., George I.M., Mushotzky R.F., Turner T.J., Yaqoob T., 1997a, *ApJ*, 477, 602
 Nandra K., George I.M., Mushotzky R.F., Turner T.J., Yaqoob T., 1997b, *ApJ*, 488, L91
 Nayakshin S., Kazanas D., Kallman T.R., 2000, *ApJ*, in press (astro-ph/9909359)
 Osterbrock D.E., Pogge R., 1985, *ApJ*, 297, 166
 Pounds K.A., Done, C., Osborne J., 1995, *MNRAS*, 277, L5
 Ross R.R., Fabian A.C., 1993, *MNRAS*, 261, 74 (RF)
 Ross R.R., Fabian A.C., Young A.J., 1999, *MNRAS*, 306, 461
 Svensson R., 1996, *A&AS*, 120, 475
 Turner T.J., George I.M., Nandra K., 1998, *ApJ*, 508, 648
 Turner T.J., George I.M., Netzer H., 1999, *ApJ*, 526, 52
 Turner T.J., George I.M., Nandra K., Turcan D., 1999, *ApJ*, 524,

667
 Vaughan S., Pounds K.A., Reeves J., Warwick R., Edelson R., 1999a, *MNRAS*, 308, L34.
 Vaughan S., Reeves J., Warwick R., Edelson R., 1999b, *MNRAS*, 309, 113.
 Zdziarski A.A., Johnson W.N., Done C., Smith D., McNaron-Brown K., 1995, *ApJ*, 438, L63
 Zdziarski A.A., Lubiński P., Smith D.A., 1999, *MNRAS*, 303, 117

This paper has been produced using the Royal Astronomical Society/Blackwell Science \LaTeX style file.

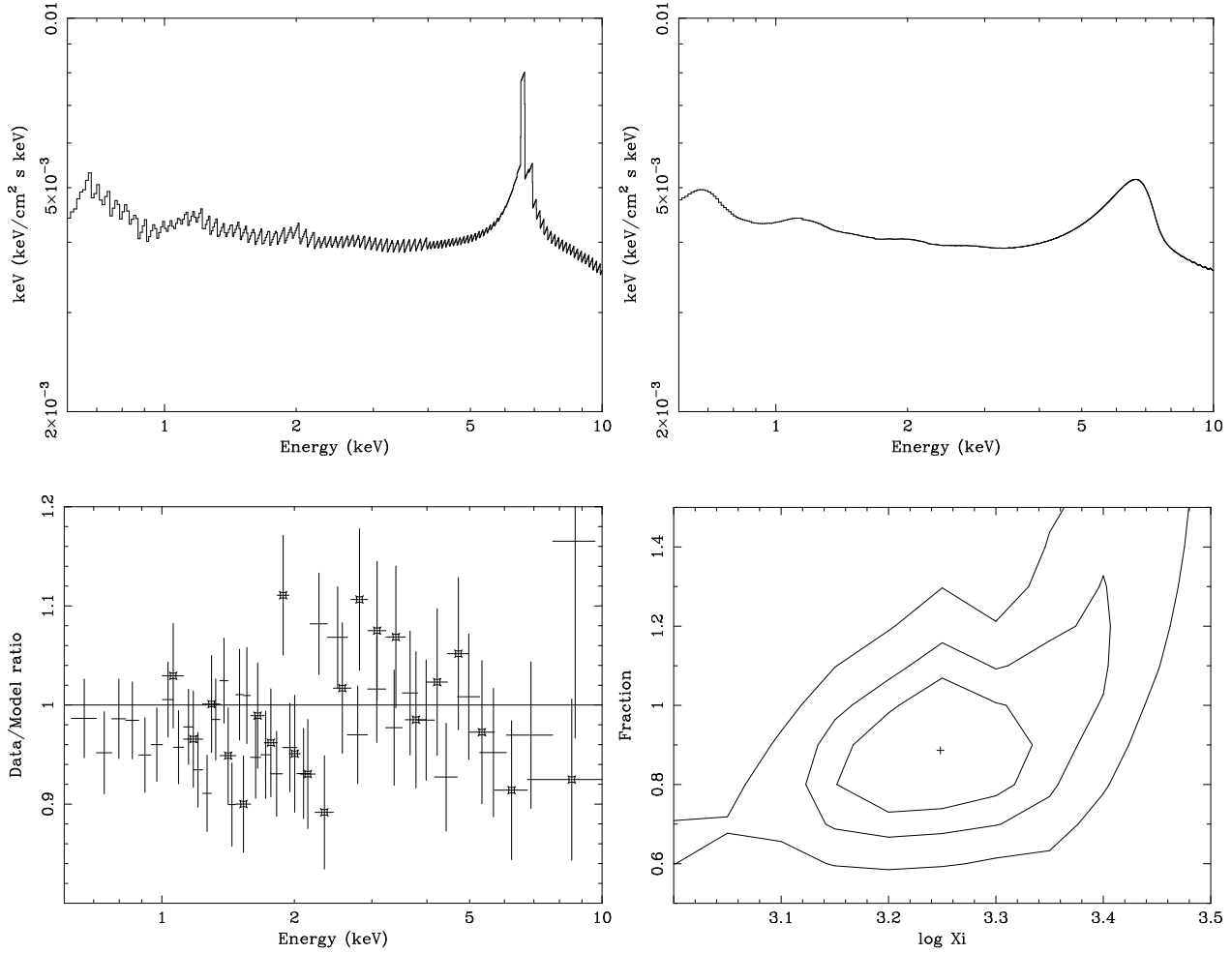


Figure 5. Results from fitting Mrk 335 with the RF ionised disc model. The top-left figure shows the best fit unblurred model: $\Gamma = 1.98$, $\log \xi = 3.34$, and $R = 0.678$. The top-right panel shows the best fit relativistically blurred model when $i = 30$ degrees: $\Gamma = 1.98$, $\log \xi = 3.25$, $R = 0.888$, $r_{min} = 6 r_g$, and $\alpha = -2.5$. The bottom left panel displays the ratio of the data to the best blurred model from the top right panel. Here, only the S0 data (no symbols) and the G2 data (open symbols) have been rebinned and plotted. Finally, the bottom right panel shows the 68, 90 and 99 per cent confidence contours around the best fitting blurred model shown in the top right panel. The position of the best fit model is denoted by the plus sign.

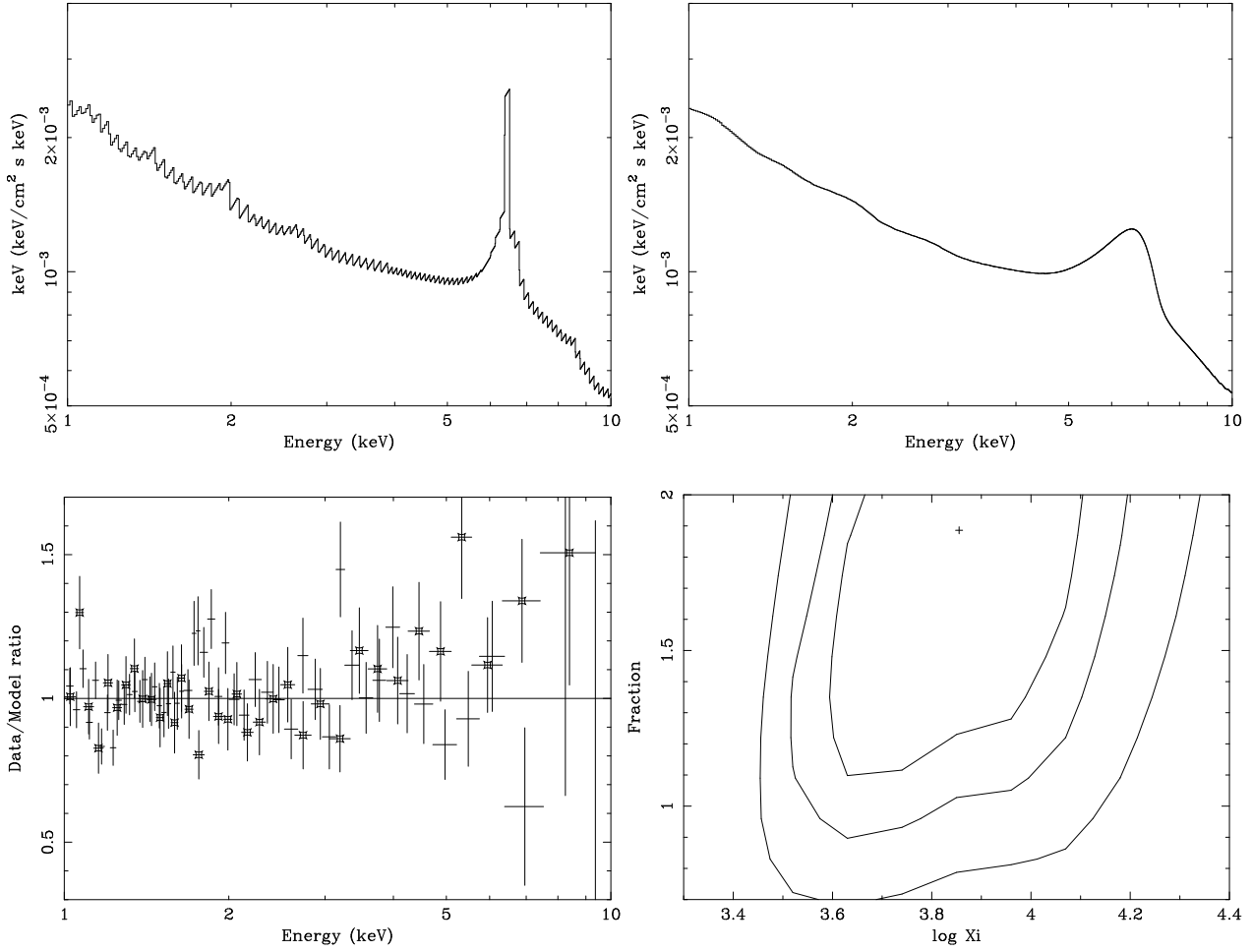


Figure 6. Results from fitting PG 1244+026 with the RF ionised disc model. The top-left figure shows the best fit unblurred model: $\Gamma = 2.43$, $\log \xi = 3.91$, and $R = 1.44$. The top-right panel shows the best fit relativistically blurred model when $i = 30$ degrees: $\Gamma = 2.42$, $\log \xi = 3.86$, $R = 1.89$, $r_{min} = 10 r_g$, and $\alpha = -2.5$. The bottom left panel displays the ratio of the data to the best blurred model from the top right panel. Here, only the S0 data (no symbols) and the G2 data (open symbols) have been rebinned and plotted. Finally, the bottom right panel shows the 68, 90 and 99 per cent confidence contours around the best fitting blurred model shown in the top right panel. The position of the best fit model is denoted by the plus sign.

Table 3. Best fit Fe K α line parameters of the sample galaxies. All values are quoted in the rest frame. Γ is the photon index, E_{Fe} is the energy centroid of the Gaussian fit in keV, σ is the width of the Gaussian also in keV and EW is the equivalent width of the line measured in eV.

Galaxy	Model	Energy Range ^a	Γ	E_{Fe}	σ	EW	χ^2/dof	χ^2_{red}
TON S 180	plaw	3–5, 7–10	2.44 ± 0.14				207/234	0.886
	plaw+gauss	3–10	2.44^f	$6.58^{+0.16}_{-0.19}$	$0.382^{+0.264}_{-0.152}$	435	275/318	0.864
PKS 0558–504	plaw	3–5, 7–10	2.24 ± 0.09				362/403	0.899
	plaw+gauss	3–10	2.24^f	$7.34^{+0.16p}_{-0.59}$	$0.985^{+0.965}_{-0.327}$	347	495/542	0.913
Ark 564	plaw	3–5, 7–20	2.57 ± 0.02				559/552	1.013
	plaw+gauss	3–20	2.57^f	$6.50^{+0.17}_{-0.25}$	$0.471^{+0.252}_{-0.238}$	174	707/723	0.978
NGC 4051	plaw	3–5, 7–10	1.84 ± 0.04				827/735	1.125
	plaw+gauss	3–10	1.84^f	$6.28^{+0.10}_{-0.11}$	$0.407^{+0.173}_{-0.227}$	255	1205/1129	1.067
Mrk 335	plaw	3–5, 7–10	$1.92^{+0.10}_{-0.12}$				203/217	0.934
	plaw+gauss	3–10	1.92^f	$6.43^{+0.12}_{-0.10}$	$0.142^{+0.174}_{-0.141}$	189	282/303	0.929
PG 1244+026	plaw	3–5, 7–10	$2.26^{+0.29}_{-0.22}$				116/123	0.936
	plaw+gauss	3–10	2.26^f	$6.66^{+0.40}_{-0.44}$	$0.556^{+0.606}_{-0.448}$	594	165/171	0.964

^a: units of keV

^f: parameter fixed at value

^{p/p}: parameter pegged at upper/lower limit

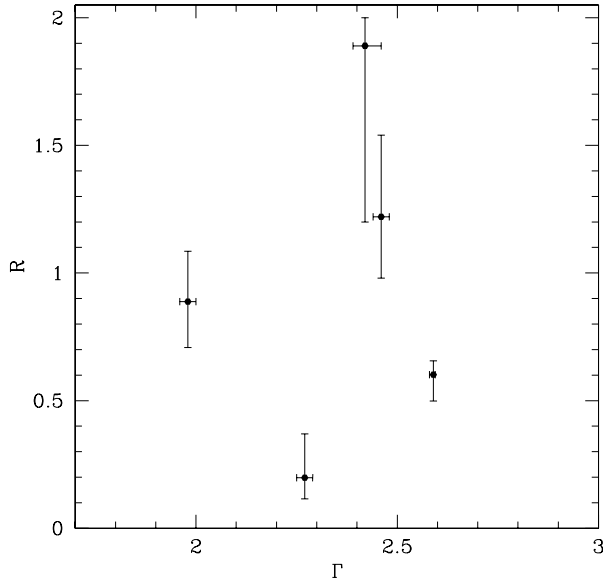


Figure 7. A plot of R vs. Γ using the data from the best fitting blurred RF model with the inclination fixed at 30 degrees. If there is a correlation it is very weak.

Table 4. Fit parameters from the alternative models considered. All values are quoted in the rest frame. Γ is the photon index and EW is the equivalent width of the Fe K α line in eV (the line energy and width are fixed with the values shown in Table 3). ξ is the ionisation parameter (in units of erg cm s $^{-1}$) of the warm absorber (for the ABSORI models) or the ionised disc (for the PEXRIV models). The value of ξ has been corrected to the same energy range as the RF models. N_H is the column density of the warm absorber in units of 10 22 cm $^{-2}$. R is the reflection fraction given by the PEXRIV models. The inclination angle of the disc has been fixed at 30 degrees for these models.

Galaxy	Model	Energy Range ^a	Γ	EW	ξ	N_H	R	χ^2/dof	χ^2_{red}
TON S 180	plaw+gauss	1–10	2.44 ^f	365				1204/862	1.396
	plaw+ABSORI+gauss		2.44 ^f	120	3180 ^{+20p} ₋₆₄₁	21.1 ^{+2.6} _{-5.1}		982/860	1.142
			2.64 ^{+0.03} _{-0.02}	600	1379 ⁺⁴⁶⁹ ₋₃₃₆	3.32 ^{+0.89} _{-0.76}		833/859	0.970
PKS 0558–504	PEXRIV+gauss		2.44 ^f	51	2794 ^{+406p} ₋₄₆₅		1.05 \pm 0.15	907/860	1.055
			2.68 ^{+0.05} _{-0.06}	235	1041 ⁺²⁴⁶ ₋₁₆₂		2.12 ^{+0.86} _{-0.63}	821/859	0.955
	plaw+gauss	1–10	2.24 ^f	148				1079/1056	1.022
Ark 564	plaw+ABSORI+gauss		2.24 ^f	52	3200 ^{+0p} ₋₆₅₉	10.9 ^{+5.2} _{-4.9}		1067/1054	1.012
			2.34 ^{+0.02} _{-0.03}	548	0.0 ^{+3200p} _{-0p}	0.02 ^{+0.30} _{-0.02p}		1012/1053	0.961
	PEXRIV+gauss		2.24 ^f	165	3199 ^{+1p} ₋₈₆₀		0.15 \pm 0.07	1035/1054	0.982
NGC 4051			2.32 \pm 0.03	450	0.0 ^{+3200p} _{-0p}		0.50 ^{+0.62} _{-0.50p}	1011/1053	0.961
	plaw+gauss	1–20	2.57 ^f	164				2232/1339	1.59
	plaw+ABSORI+gauss		2.57 ^f	35	3200 ^{+0p} ₋₁₄₅	6.9 ^{+0.6} _{-0.5}		1776/1337	1.328
Mrk 335			2.71 \pm 0.01	233	1032 ⁺²¹² ₋₁₂₄	1.8 \pm 0.2		1467/1336	1.098
	PEXRIV+gauss		2.57 ^f	0.0	3200 ^{+0.0p} ₋₁₈₄		0.53 ^{+0.03} _{-0.06}	1635/1337	1.223
			2.73 \pm 0.02	0.0	968 ⁺¹⁴⁹ ₋₁₂₆		1.4 \pm 0.2	1416/1336	1.060
PG 1244+026	plaw+gauss	0.5–10	1.84 ^f	40				7713/1835	4.203
	plaw+ABSORI+gauss		1.84 ^f	0.0	1107	73		5635/1833	3.074
			2.031 \pm 0.006	316	3200 ^{+0p} ₋₁₃₆	99 \pm 1		3351/1832	1.829
Mrk 335	PEXRIV+gauss		1.84 ^f	0.0	668		1.1	3945/1833	2.152
			2.11 ^{+0.02} _{-0.01}	27	83.9 ^{+3.2} _{-4.6}		2.4 ^{+0.3} _{-0.2}	2429/1832	1.326
	plaw+gauss	0.6–10	1.92 ^f	87				1328/735	1.807
PG 1244+026	plaw+ABSORI+gauss		1.92 ^f	0.0	705 ⁺¹⁸¹ ₋₁₄₄	22.9 ^{+8.6} _{-6.6}		1183/733	1.614
			2.15 \pm 0.02	246	157 ⁺⁵⁹ ₋₃₃	2.8 ^{+0.8} _{-0.7}		804/732	1.099
	PEXRIV+gauss		1.92 ^f	0.0	666 ⁺¹⁴⁸ ₋₁₁₇		0.84 ^{+0.11} _{-0.12}	1034/733	1.411
Mrk 335			2.14 \pm 0.04	140	138 ⁺⁸¹ ₋₄₁		1.26 ^{+0.58} _{-0.39}	792/732	1.082
	plaw+gauss	1–10	2.26 ^f	59				947/519	1.824
	plaw+ABSORI+gauss		2.26 ^f	0.0	3200 ^{+0p} ₋₁₀₈	77 ⁺⁸ ₋₁₂		766/517	1.482
PG 1244+026			2.71 ^{+0.08} _{-0.06}	1400	567 ⁺⁵⁹⁴ ₋₂₀₀	1.1 ^{+0.54} _{-0.55}		556/516	1.077
	PEXRIV+gauss		2.26 ^f	0.0	3199 ^{+1p} ₋₂₉₅		1.8 ^{+0.5} _{-0.3}	723/517	1.399
			2.80 ^{+0.09} _{-0.07}	336	530 ⁺²¹⁹ ₋₃₅₅		4.1 ^{+3.0} _{-1.4}	540/516	1.046

^a: units of keV

^f: parameter fixed at value

^p/_p: parameter pegged at upper/lower limit

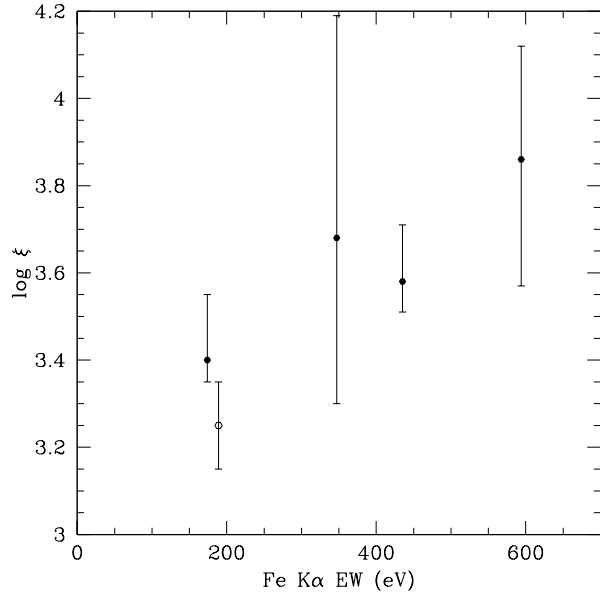


Figure 8. Plot of $\log \xi$ from the best fitting blurred RF models (with the inclination fixed at 30 degrees) versus Fe K α EW, excluding NGC 4051. The source with $\Gamma < 2.0$ (Mrk 335) is plotted with an open symbol.